

Article

E-Band InAs Quantum Dot Micro-Disk Laser with Metamorphic InGaAs Layers Grown on GaAs/Si (001) Substrate

Wenqian Liang^{1,2}, Wenqi Wei² , Dong Han³ , Ming Ming^{2,3}, Jieyin Zhang², Zihao Wang^{2,3} , Xinding Zhang^{1,*}, Ting Wang^{2,3,*}  and Jianjun Zhang^{2,3}

¹ School of Physics, South China Normal University, Guangzhou 510631, China

² Songshan Lake Materials Laboratory, Dongguan 523808, China; weiwenqi@sslslab.org.cn (W.W.)

³ Beijing National Laboratory for Condensed Matter Physics, Institute of Physics, Chinese Academy of Sciences, Beijing 100190, China

* Correspondence: xdzhang@scnu.edu.cn (X.Z.); wangting@iphy.ac.cn (T.W.)

Abstract: The direct growth of III-V quantum dot (QD) lasers on silicon substrate has been rapidly developing over the past decade and has been recognized as a promising method for achieving on-chip light sources in photonic integrated circuits (PICs). Up to date, O- and C/L-bands InAs QD lasers on Si have been extensively investigated, but as an extended telecommunication wavelength, the E-band QD lasers directly grown on Si substrates are not available yet. Here, we demonstrate the first E-band (1365 nm) InAs QD micro-disk lasers epitaxially grown on Si (001) substrates by using a III-V/IV hybrid dual-chamber molecular beam epitaxy (MBE) system. The micro-disk laser device on Si was characterized with an optical threshold power of 0.424 mW and quality factor (Q) of 1727.2 at 200 K. The results presented here indicate a path to on-chip silicon photonic telecom-transmitters.

Keywords: III-V on silicon; micro-disk lasers; E-band quantum dots; photonic integrated circuits; molecular beam epitaxy



Citation: Liang, W.; Wei, W.; Han, D.; Ming, M.; Zhang, J.; Wang, Z.; Zhang, X.; Wang, T.; Zhang, J. E-Band InAs Quantum Dot Micro-Disk Laser with Metamorphic InGaAs Layers Grown on GaAs/Si (001) Substrate. *Materials* **2024**, *17*, 1916. <https://doi.org/10.3390/ma17081916>

Academic Editor: Albena Paskaleva

Received: 13 March 2024

Revised: 15 April 2024

Accepted: 19 April 2024

Published: 21 April 2024



Copyright: © 2024 by the authors. Licensee MDPI, Basel, Switzerland. This article is an open access article distributed under the terms and conditions of the Creative Commons Attribution (CC BY) license (<https://creativecommons.org/licenses/by/4.0/>).

1. Introduction

The heterogeneous integration of III-V functional devices on silicon substrates is an important research field in future applications of information and communication. With the rapid development of silicon photonics, III-V quantum dot (QD) lasers integrated on CMOS-compatible silicon substrates have been becoming an essential component for photonic integrated chips (PICs) [1–4]. Over the past decade, a lot of research related to directly epitaxial growing III-V QD lasers on silicon and SOI substrates has been demonstrated, such as Fabry–Perot (FP) lasers [5–11], distributed feedback (DFB) lasers [12–15] and micro-cavity lasers [16–20]. However, almost all III-V lasers involve the O-band (original band: 1260–1360 nm) or C-band (conventional band: 1530–1565 nm) wavelengths, which are the low-loss wavelength regions used in traditional optical fibers for wavelength division multiplexing (WDM). In order to extend the optical communication window, the E-band (1360–1460 nm) wavelength has also been developed and used in optical fibers (ITU-T G.652.D) [21], which are fabricated by the dehydration process to reduce the relatively high loss from water absorption [22]. In previous research, several attempts have been made towards E-band III-V lasers, such as InGaAsP multi-quantum-well (MQW) lasers on InP [23], GaInNAs MQW lasers on GaAs [24] and InAs QD lasers on metamorphic InGaAs [25], but direct epitaxially grown E-band III-V lasers on Si substrates have not been reported yet. Additionally, microcavity lasers own unique advantages such as a small footprint, low power consumption and a high-quality (Q) factor, which can be used as compact on-chip light sources in PICs or sensing techniques.

In this work, we demonstrated direct epitaxially grown E-band InAs/InGaAs QD micro-disk lasers on Si (001) substrates. The step-graded metamorphic InGaAs buffer

layers are implemented here to extend the emission wavelength of InAs QDs to the E-band [26–29], while the QD properties are also characterized by atomic force microscopy (AFM), cross-sectional transmission electron microscopy (TEM) and photoluminescence (PL) measurements. Furthermore, the fabricated InAs/InGaAs QD micro-disk laser on Si with a diameter of 4 μm is measured with an emission wavelength of 1364.5 nm and a threshold power of 0.424 mW. The results presented here pave a promising way for the epitaxial integration of III-V light sources on a silicon photonic platform.

2. Experimental Details

2.1. Materials' Growth

Epitaxial growth of the sample was performed by a solid-source III-V/IV hybrid dual-chamber molecular beam epitaxy (MBE) system. A standard 8-inch Si (001) substrate was patterned with U-shaped grating structures along the [110] direction in CMOS process line. The U-shaped gratings with a period of 360 nm and a ridge width of approximately 140 nm were fabricated by deep ultraviolet (DUV) photolithography and dry etching process. After immersion in diluted hydrofluoric acid (HF) solution to remove the native oxide layer, the patterned Si (001) substrate was loaded in MBE chamber and the silicon homoepitaxial growth was conducted to construct (111)-faceted silicon hollow sawtooth structures on the U-shaped gratings. Then, the (111)-faceted silicon hollow substrate was transferred into the III-V MBE chamber for in situ III-V hybrid growth. As the schematic diagram shows in Figure 1, approximately 2100 nm thick III-V buffer layers were grown to achieve a smooth GaAs layer with low defect density on Si (001) substrate.

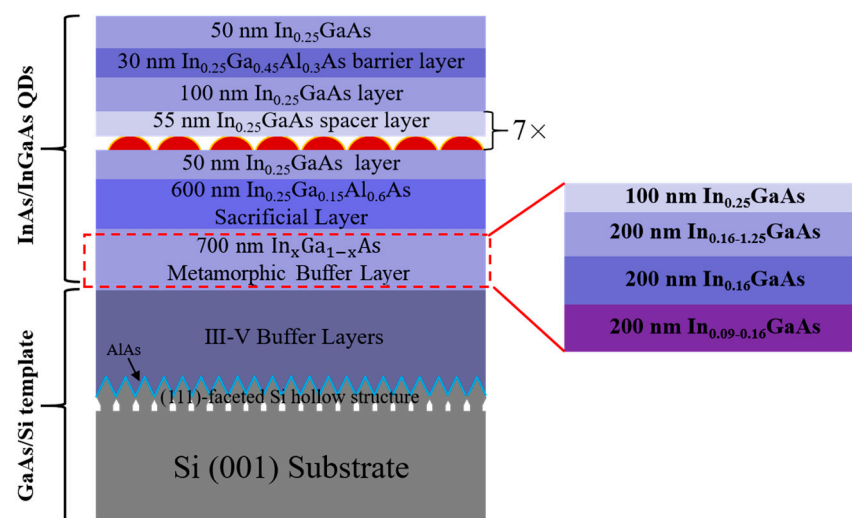


Figure 1. Schematic diagram of the E-band InAs QD micro-disk laser sample epitaxially grown on GaAs/Si (001) template with a 7-layer InAs/InGaAs QDs as active region. The right diagram shows the detailed structure of InGaAs metamorphic buffer layer grown by step-graded method.

Here, a 10 nm AlAs nucleation layer and a 30 nm GaAs low-temperature buffer layer were first deposited at 380 $^{\circ}\text{C}$ to form a high-quality interface at Si (111) facets, as shown in Figure 1. The III-V buffer layers mainly consisted of 2 periods of InGaAs/GaAs and 2 repeats of InAlAs/GaAs quantum wells (QWs), both of which acted as dislocation filter layers (DFLs) to reduce the threading dislocation density (TDD) to the order of $10^6/\text{cm}^2$ [8,26,30]. Each of the DFLs included 5 periods of 10 nm-InGa(Al)As/10 nm-GaAs and 200 nm GaAs spacer layer. Lastly, the GaAs/AlGaAs superlattices (SLs) were also deposited to smooth the surface of the III-V buffer layers. The structural and growth details of the 2100 nm III-V buffer layers on Si can be found in our previous research [26,30].

To extend the emission wavelength of InAs QDs, step-graded metamorphic InGaAs buffer layers were introduced, as described in the earlier work [16,26]. Figure 1 schematically shows the whole structure of the E-band InAs QD micro-disk laser sample. Here,

in order to achieve the E-band emission, an InGaAs layer with 25% indium content was grown on a 700 nm thick InGaAs metamorphic buffer layer grown by the step-graded epitaxial growth method ranging from $\text{In}_{0.09}\text{Ga}_{0.91}\text{As}$ to $\text{In}_{0.25}\text{Ga}_{0.75}\text{As}$. The detailed structure of the metamorphic buffer is also shown in Figure 1. Each layer of metamorphic InGaAs was 200 nm and grown at a low temperature of 380 °C to suppress the lattice-misfit-induced defects. Then, the thermal cycle annealing (TCA) process was introduced at an optimum temperature of 510 °C for high crystal quality and flat InGaAs layers [16]. Seven layers of InAs/ $\text{In}_{0.25}\text{Ga}_{0.75}\text{As}$ QDs as active region were grown on the 600 nm thick $\text{In}_{0.25}\text{Ga}_{0.15}\text{Al}_{0.6}\text{As}$ sacrificial layer. Each layer of the InAs QDs consisted of 3.1 monolayer (ML) InAs grown at 445 °C, which was capped by a 10 nm low-temperature $\text{In}_{0.25}\text{Ga}_{0.75}\text{As}$ layer (445 °C) and separated by a 45 nm $\text{In}_{0.25}\text{Ga}_{0.75}\text{As}$ spacer layer grown at higher temperature of 500 °C. The whole InAs/ $\text{In}_{0.25}\text{Ga}_{0.75}\text{As}$ QD active region was sandwiched by 50 nm and 100 nm lower and upper InGaAs buffer layers, respectively. A 30 nm $\text{In}_{0.25}\text{Ga}_{0.45}\text{Al}_{0.3}\text{As}$ layer was also grown as a barrier layer to increase the quantum efficiency of the lasers. Lastly, a 50 nm $\text{In}_{0.25}\text{Ga}_{0.75}\text{As}$ buffer layer was grown to achieve the smooth sample surface.

2.2. Material Characterizations

A sample with a five-layer of E-band InAs/ $\text{In}_{0.25}\text{Ga}_{0.75}\text{As}$ QD active region and surface InAs QDs was grown on GaAs/Si substrate for material characterizations. The bright-field cross-sectional TEM measurements of the sample were conducted to characterize the crystal quality, as shown in Figure 2.

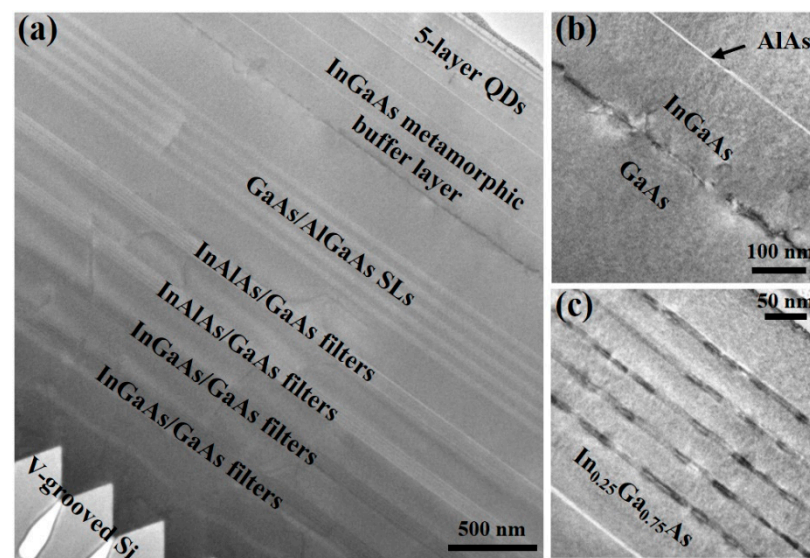


Figure 2. (a) Bright-field cross-sectional TEM image of a five-layer of E-band InAs/ $\text{In}_{0.25}\text{Ga}_{0.75}\text{As}$ QDs grown on $\text{In}_{0.25}\text{Ga}_{0.75}\text{As}/\text{GaAs}/\text{Si}$ substrate. (b,c) show the zoomed-in TEM images at the $\text{In}_{0.25}\text{Ga}_{0.75}\text{As}/\text{GaAs}$ interface and InAs QD active region, respectively.

Benefiting from the homoepitaxially formed (111)-faceted sawtooth structures and the $\text{InGa}(\text{Al})\text{As}/\text{GaAs}$ DFLs, the defects were mostly confined to the GaAs/Si interface and III-V buffer region, without propagating into the upper region shown in Figure 2a. Smooth GaAs surface with approximately 1 nm roughness and $5 \times 10^6/\text{cm}^2$ TDD can be obtained on these Si (001) substrates [26]. Figure 2b shows the zoomed-in TEM image of the interface between $\text{In}_{0.25}\text{Ga}_{0.75}\text{As}$ metamorphic buffer layer and GaAs layer, which indicates that most of the lattice-mismatch-induced defects are confined to the interface due to the low-temperature growth method at 380 °C. The 3 nm thick AlAs layers between $\text{In}_{0.25}\text{Ga}_{0.75}\text{As}$ metamorphic buffer layers can be also obviously distinguished due to the SEM contrast, which were grown to prevent the indium desorption at a high annealing temperature of 510 °C. Figure 2c shows the zoomed-in TEM image of the five layers of InAs/ $\text{In}_{0.25}\text{Ga}_{0.75}\text{As}$ QDs, and no obvious defects are observed in the active region.

To accurately characterize the surface morphology of InAs/In_{0.25}Ga_{0.75}As QDs, AFM measurements of the surface QDs were conducted by a Bruker Dimension Icon instrument with a silicon tip coated with aluminum (Model: RTESPA-150) in the tapping mode on both GaAs (001) and GaAs/Si (001) substrates. Figure 3a,b show the diameter and height histograms of the surface InAs QDs on GaAs (001) and GaAs/Si (001) substrates, respectively.

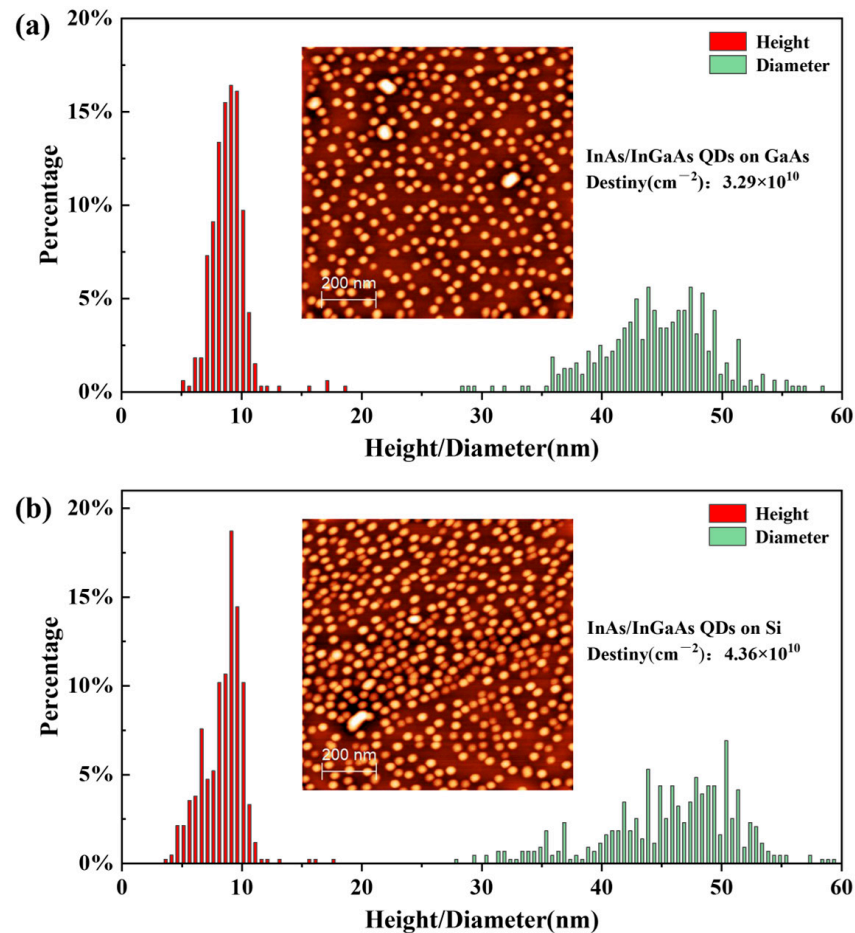


Figure 3. Diameter and height histograms of the surface InAs/InGaAs QDs on (a) GaAs (001) substrate and (b) GaAs/Si (001) substrate, respectively. Insets in (a,b) show the $1 \times 1 \mu\text{m}^2$ AFM images of the surface InAs/InGaAs QDs on these two substrates.

The insets show the $1 \times 1 \mu\text{m}^2$ AFM images of the InAs/InGaAs QDs on these two substrates with dot densities of $3.29 \times 10^{10}/\text{cm}^2$ and $4.36 \times 10^{10}/\text{cm}^2$, respectively. The average height and diameter of the QDs on GaAs (001) are 9.001 nm and 44.835 nm with the mean square error (MSE) of 1.483 nm and 5.753 nm, respectively. As a comparison, the average height and diameter of the QDs on GaAs/Si (001) substrate were also analyzed with values of 8.682 nm (MSE: 1.723 nm) and 45.728 nm (MSE: 7.409 nm), which are similar to those on GaAs (001) substrate. Additionally, a slightly elongated shape of the QDs on Si (001) substrate can be observed from the AFM image, which is caused by the unevenness of the InGaAs/GaAs/Si surface [16,26]. Compared with the O-band InAs/GaAs QDs reported in previous work [26], the E-band InAs/InGaAs QDs own larger sizes due to the smaller mismatch between InAs QD and InGaAs layers than that between InAs QD and GaAs layer. Moreover, the inset in Figure 4a shows the cross-sectional TEM image of a buried InAs/InGaAs QD, indicating a 7.5 nm height and 50 nm diameter.

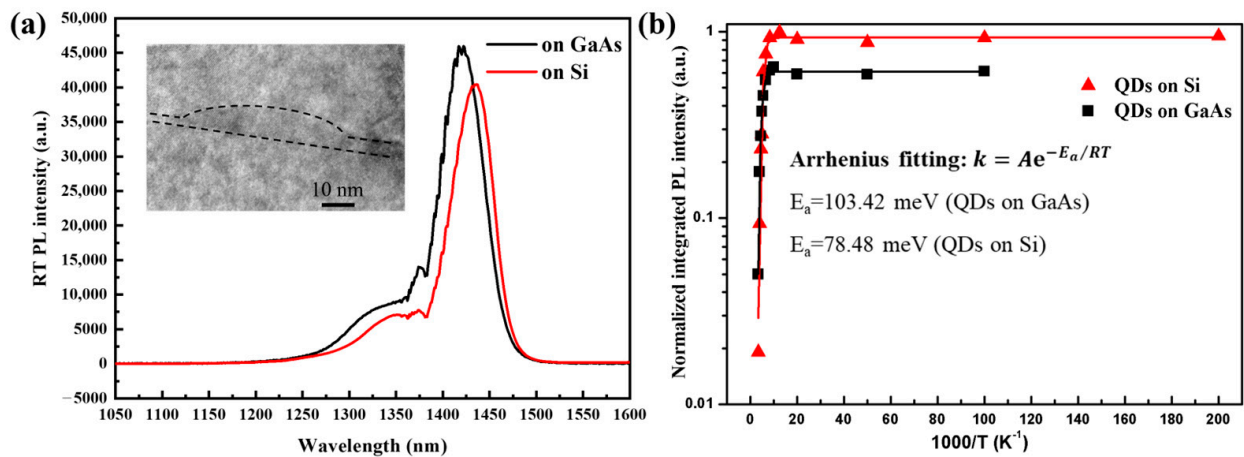


Figure 4. (a) Room-temperature PL spectra of InAs/InGaAs QDs on GaAs (001) and GaAs/Si (001) substrates, respectively. Inset: the cross-sectional TEM image of a buried InAs/InGaAs QD on InGaAs/GaAs/Si (001) substrate. (b) Arrhenius plots of temperature-dependent IPLI of the InAs QDs on GaAs and Si, respectively.

In Figure 4a, room-temperature (RT) PL spectra of the InAs/InGaAs QDs on both GaAs (001) and Si (001) substrates are measured with a continuous-wave (CW) 532 nm solid-state pumping laser. E-band (1434.7 nm) PL peak emission with a full width at half maximum (FWHM) of 31.4 meV can be observed from the InAs/InGaAs QDs on Si (001). For InAs/InGaAs QDs on GaAs, the PL central wavelength and FWHM are 1421 nm and 33.5 meV, respectively. As shown in Figure 4a, a small shoulder can be distinguished from both of the spectra, which arises from the excited state of the QDs. Furthermore, the obvious noise-like PL spectra around 1400 nm can be also observed, which are caused by the defect of the gratings with the grating density of 600 grooves/mm used in the HORIBA monochromator for PL collection [16]. Moreover, the PL peak intensity of InAs/InGaAs QDs on Si substrate is about 87% of that on GaAs substrate, indicating that the Si-based InAs QDs own good QD quality and uniformity such as those on GaAs substrate. Additionally, more optical properties of the InAs QDs grown on these two substrates were investigated by the temperature-dependent PL measurements. Figure 4b shows the normalized integrated PL intensity (IPLI) plots of the two samples with a reciprocal temperature as the abscissa. The black and red curves are the Arrhenius fitting results of the experimental data by using the formula $k = Ae^{-E_a/RT}$ [31]. With the increase in temperature, the decrease in IPLI can be observed from the plot due to the thermal escape of the carriers from the ground state of QDs to surrounding layers. Here, the thermal activation energies (E_a) of the two samples can be calculated as the values of 103.42 meV (standard error: 6.27) and 78.48 meV (standard error: 2.29), respectively, for the InAs QDs on GaAs (001) and Si (001) substrates, which are almost the same as the values reported previously [26]. For the sample on Si substrate, the thermal activation energy of 78.48 meV is significantly lower than that on GaAs substrate, which is probably due to increased non-radiative recombination from the defects on GaAs/Si platform than that on native GaAs (001) substrate.

2.3. Device Fabrication

Figure 5a,b show the schematic diagram and scanning electron microscopy (SEM) image of the silicon-based micro-disk laser with a diameter of 4 μm by using the sample as shown in Figure 1, which contains 7 layers of InAs/InGaAs QDs as the active region for high optical gain.

The micro-disk structure was fabricated by a two-step etching method [16]. First, the silica beads with diameter of 4 μm were scattered on the surface of the sample, acting as the hard mask for mesa etching. After dry etching by ICP (inductively coupled plasma) process, the sample with pillar mesas was dipped in a 50% diluted HCl solution for

selective wet etching of 600 nm InGaAlAs sacrificial layers to construct supporting pillar as shown in Figure 5a. The detailed fabrication process can be referred to in our previous work [16]. Figure 5b shows the SEM image of a fabricated disk laser on Si substrate, which presents a clean and smooth sidewall of the disk. By optimizing the wet etching process, a slender supporting pillar can be achieved, which can ensure the high optical confinement of the micro-disk.

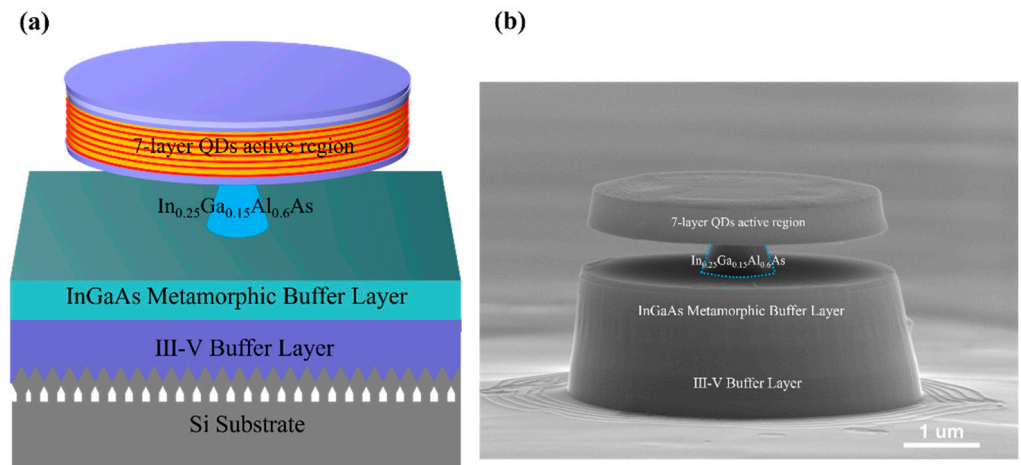


Figure 5. (a) Schematic diagram of an E-band micro-disk laser on GaAs/Si (001) substrate with seven layers of InAs/InGaAs QDs as active region and 600 nm InGaAlAs sacrificial layer. (b) SEM image of a fabricated micro-disk laser on Si with a diameter of 4 μm .

3. Results and Discussions

For characterizations of the device properties, the micro-disk laser sample was mounted in liquid-helium-cooled cryostat and measured under a micro-photoluminescent (μPL) system with a CW 532 nm solid-state pumping laser. All the optical properties of the laser were characterized at a temperature of 200 K. Figure 6a,b show the relationship of the laser output intensity as a function of pumping power (L-L curve) and the power-dependent emission spectra of the laser, respectively.

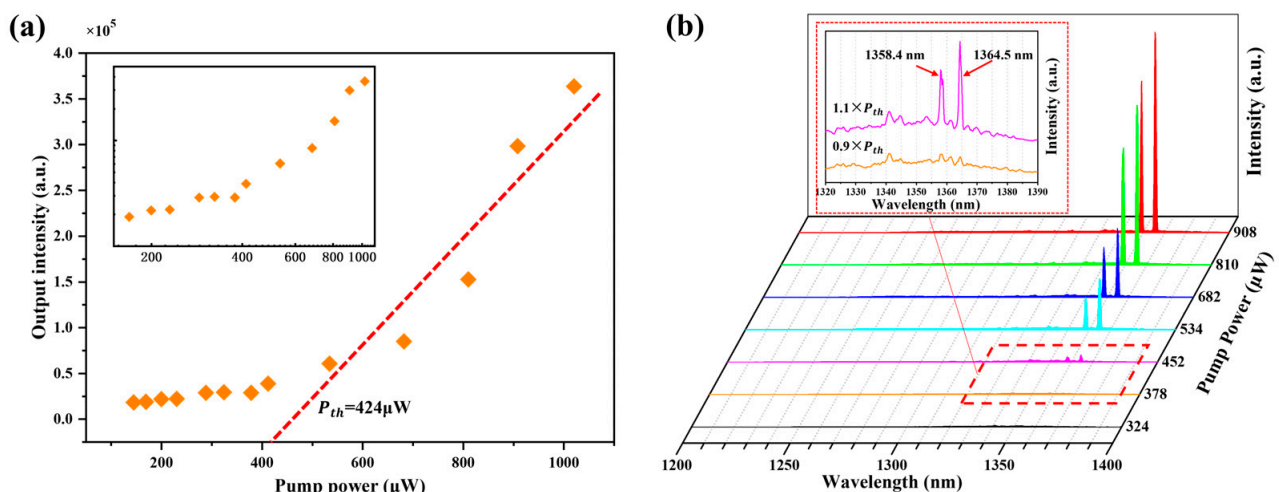


Figure 6. (a) The output intensity of the micro-disk laser on Si substrate versus the effective pumping power (L-L curve). Inset: the log-log scale plot of the non-linear L-L curve. (b) Pumping-power-dependent lasing spectra of the laser device. Inset: zoomed-in spectra collected at the pumping power below and above threshold.

The orange square symbols in Figure 6a represent the experimental data, fitted by a red dotted line. Here, the threshold power of this micro-disk laser on Si is calculated as a value

of 0.424 mW (Standard error: 0.057) from the L-L curve. The inset of Figure 6a presents the log-log scale plot of the non-linear L-L curve, showing an “S” shape, which demonstrates three modes of nonlinear transition of lasing phenomena: spontaneous emission, amplified spontaneous emission and laser oscillation [32]. Figure 6b shows the spectral evolution of the micro-disk laser with an increase in the pumping power from 0.324 mW to 0.908 mW. At a low pumping power, broad spontaneous emission spectra were observed. As the pumping power gradually increased, obvious sharp peaks of the micro-disk laser on the Si substrate occurred. The inset of Figure 6b shows the zoomed-in spectra of the laser below ($0.9 \times P_{th}$) and above ($1.1 \times P_{th}$) the threshold power, displaying that the dominant lasing wavelength peaked at 1364.5 nm and another one at 1358.4 nm. Here, an obvious blue shift in the lasing peak (1364.5 nm) can be found referring to the RT PL spectrum of the InAs QDs on Si (peak: 1434.7 nm), which is caused by the typical temperature dependence of the peak position for semiconductor materials [33,34].

Figure 7a indicates the zoomed-in spectra of the Si-based micro-disk laser at increasing pumping power, which shows an obvious red shift in the two peak wavelengths due to the thermal effects from a pumping laser.

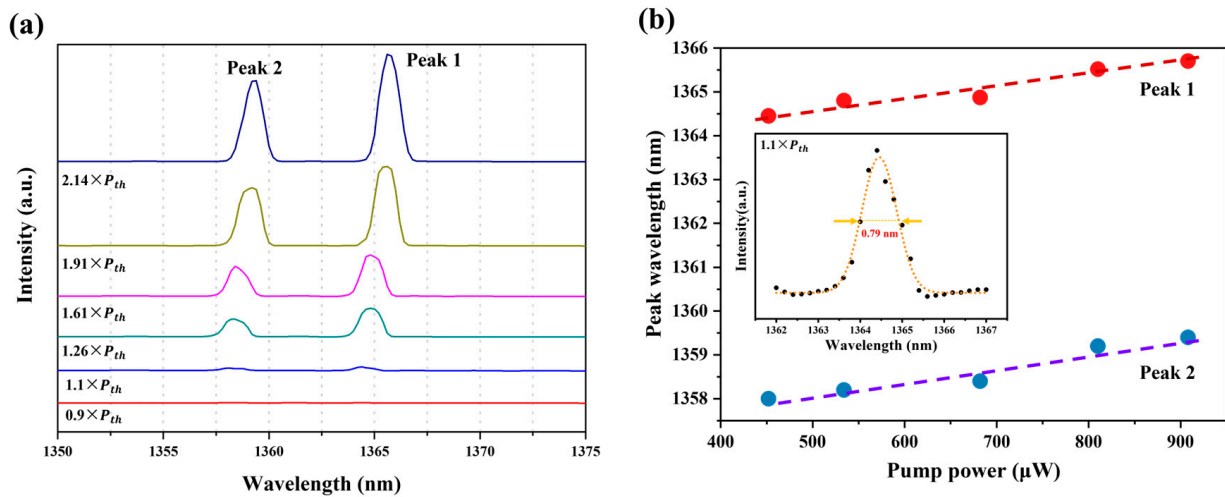


Figure 7. (a) Zoomed-in spectra of the micro-disk laser on the Si substrate at the increasing pumping power, indicating multi-peak lasing property. (b) The relationship of the two lasing peak wavelengths as a function of the pumping power. Inset: zoomed-in spectrum of the dominant peak (1364.5 nm) from the laser fitting by Lorentzian curve at $1.1 \times P_{th}$, showing a 0.79 nm linewidth.

Figure 7b shows the relationship of the two lasing peak wavelengths as a function of the pumping powers. The red circle symbols display the experimental data of dominant emission peak (Peak 1), extracted from Figure 7a. The shifting rate of Peak 1 is calculated with a value of 2.69 nm/mW (Standard error: 0.39) from the fitting results in Figure 7b, which is slightly smaller than that (3.2 nm/mW with standard error of 0.46) of Peak 2. The inset of Figure 7b displays the zoomed-in Peak 1 spectrum of the micro-disk laser on Si at the pumping power slightly above the threshold power ($1.1 \times P_{th}$), and the experimental data are fitted by a Lorentzian fitting line shape (orange curve). Here, the cavity quality factor (Q) of the micro-disk can be calculated with $Q = \lambda_{cav} / \Delta\lambda_{cav}$, in which $\Delta\lambda_{cav}$ is the linewidth with a value of 0.79 nm obtained from Lorentzian fitting curve and λ_{cav} is the dominant lasing peak of 1364.5 nm. The Q factor of the E-band micro-disk laser on Si (001) substrate is obtained as a value of 1727.2, which is a little higher than that (1626) of the S-band micro-disk laser on SOI substrates [16]. This is probably due to the lower defect density of the $\text{In}_{0.25}\text{Ga}_{0.75}\text{As}$ on GaAs/Si (001) substrates used here than that of $\text{In}_{0.35}\text{Ga}_{0.65}\text{As}$ on the GaAs/SOI platforms for S-band lasing.

4. Conclusions

In summary, we have successfully demonstrated the optically pumped, direct epitaxially grown E-band InAs QD micro-disk lasers on GaAs/Si (001) substrates by using the In_{0.25}Ga_{0.75}As metamorphic buffer layer. The crystal quality and optical properties of the E-band InAs/InGaAs QDs on Si (001) are investigated and discussed. The fabricated micro-disk laser with a 4 μm diameter presents a low threshold power of 0.424 mW and a Q factor of 1727.2 at 200 K. In order to further enhance the performance of the device, our forthcoming efforts will concentrate on optimizing the epitaxial growth parameters and structures, aiming to diminish the dislocation densities and improve the crystal quality. Overall, the results presented here provide a promising solution to realize on-chip telecom light sources not only for silicon photonic integration but also for potential sensing applications.

Author Contributions: Methodology, W.L. and W.W.; validation, W.L.; resources, X.Z., Z.W., T.W. and J.Z. (Jianjun Zhang); data curation, M.M., J.Z. (Jieyin Zhang) and D.H.; writing—original draft preparation, W.L.; writing—review and editing, W.W., X.Z. and J.Z. (Jianjun Zhang); supervision, T.W. and J.Z. (Jianjun Zhang). All authors have read and agreed to the published version of the manuscript.

Funding: This research was funded by the National Key Research and Development Program of China (2021YFB2800403), National Natural Science Foundation of China (Grant No. 62225407, 61975230, 62005308, 12274449, 12304100), Innovation Program for Quantum Science and Technology (No. 2021ZD0302300) and Songshan Lake Materials Laboratory (No. XMY2023002). Ting Wang was supported by the Youth Innovation Promotion Association of CAS (Y2022005).

Institutional Review Board Statement: Not applicable.

Informed Consent Statement: Not applicable.

Data Availability Statement: Data are contained within the article.

Acknowledgments: The authors would like to acknowledge Songshan Lake Materials Laboratory and Beijing National Laboratory for Condensed Matter Physics for providing the research background and experimental instruments and guidance.

Conflicts of Interest: The authors declare no conflicts of interest.

References

1. Asghari, M.; Krishnamoorthy, A.V. Silicon photonics: Energy-efficient communication. *Nat. Photonics* **2011**, *5*, 268–270. [[CrossRef](#)]
2. Hu, Y.; Liang, D.; Mukherjee, K.; Li, Y.; Zhang, C.; Kurczveil, G.; Huang, X.; Beausoleil, R.G. III/V-on-Si MQW lasers by using a novel photonic integration method of regrowth on a bonding template. *Light Sci. Appl.* **2019**, *8*, 93. [[CrossRef](#)] [[PubMed](#)]
3. Hu, Y.; Liang, D.; Beausoleil, R.G. An advanced III-V-on-silicon photonic integration platform. *Opto-Electron. Adv.* **2021**, *4*, 200094. [[CrossRef](#)]
4. Shekhar, S.; Bogaerts, W.; Chrostowski, L.; Bowers, J.E.; Hochberg, M.; Soref, R.; Shastri, B.J. Roadmapping the next generation of silicon photonics. *Nat. Commun.* **2024**, *15*, 751. [[CrossRef](#)] [[PubMed](#)]
5. Chen, S.; Li, W.; Wu, J.; Jiang, Q.; Tang, M.; Shutts, S.; Elliott, S.N.; Sobiesierski, A.D.; Seeds, A.J.; Ross, I.M. Electrically pumped continuous-wave III-V quantum dot lasers on silicon. *Nat. Photonics* **2016**, *10*, 307–311. [[CrossRef](#)]
6. Jhang, Y.H.; Mochida, R.; Tanabe, K.; Takemasa, K.; Sugawara, M.; Iwamoto, S.; Arakawa, Y. Direct modulation of 1.3 μm quantum dot lasers on silicon at 60 °C. *Opt. Express* **2016**, *24*, 18428–18435. [[CrossRef](#)] [[PubMed](#)]
7. Liu, A.Y.; Peters, J.D.; Huang, X.; Jung, D.; Norman, J.C.; Lee, M.L.; Gossard, A.C.; Bowers, J.E. Electrically pumped continuous-wave 1.3 μm quantum-dot lasers epitaxially grown on on-axis (001) GaP/Si. *Opt. Lett.* **2017**, *42*, 338–341. [[CrossRef](#)] [[PubMed](#)]
8. Wei, W.Q.; Feng, Q.; Guo, J.J.; Guo, M.C.; Wang, J.H.; Wang, Z.H.; Wang, T.; Zhang, J.J. InAs/GaAs quantum dot narrow ridge lasers epitaxially grown on SOI substrates for silicon photonic integration. *Opt. Express* **2020**, *28*, 26555–26563. [[CrossRef](#)] [[PubMed](#)]
9. Lv, Z.; Wang, S.; Wang, S.; Chai, H.; Meng, L.; Yang, X.; Yang, T. Ultra-high thermal stability InAs/GaAs quantum dot lasers grown on on-axis Si (001) with a record-high continuous-wave operating temperature of 150 °C. *Opt. Express* **2023**, *31*, 24173–24182. [[CrossRef](#)]
10. Wei, W.Q.; He, A.; Yang, B.; Wang, Z.H.; Huang, J.Z.; Han, D.; Ming, M.; Guo, X.; Su, Y.; Zhang, J.J.; et al. Monolithic integration of embedded III-V lasers on SOI. *Light Sci. Appl.* **2023**, *12*, 84. [[CrossRef](#)]
11. Feng, K.; Shang, C.; Hughes, E.; Clark, A.; Koscica, R.; Ludewig, P.; Haramé, D.; Bowers, J. Quantum Dot Lasers Directly Grown on 300 mm Si Wafers: Planar and In-Pocket. *Photonics* **2023**, *10*, 534. [[CrossRef](#)]

12. Tian, B.; Wang, Z.; Pantouvaki, M.; Absil, P.; Van Campenhout, J.; Merckling, C.; Van Thourhout, D. Room Temperature O-band DFB Laser Array Directly Grown on (001) Silicon. *Nano Lett.* **2017**, *17*, 559–564. [[CrossRef](#)]
13. Wang, Y.; Chen, S.; Yu, Y.; Zhou, L.; Liu, L.; Yang, C.; Liao, M.; Tang, M.; Wu, J.; Li, W.; et al. Monolithic quantum-dot distributed feedback laser array on silicon. *Optica* **2018**, *5*, 528–533. [[CrossRef](#)]
14. Shi, Y.; Baryshnikova, M.; Mols, Y.; Pantouvaki, M.; Van Campenhout, J.; Kunert, B.; Van Thourhout, D. Loss-Coupled DFB Nano-ridge Laser Monolithically Grown on a Standard 300-mm Si Wafer. *Opt. Express* **2019**, *29*, 14649–14657. [[CrossRef](#)]
15. Wan, Y.; Norman, J.C.; Tong, Y.; Kennedy, M.J.; He, W.; Selvidge, J.; Shang, C.; Dumont, M.; Malik, A.; Tsang, H.K.; et al. 1.3 μm Quantum Dot-Distributed Feedback Lasers Directly Grown on (001) Si. *Laser Photonics Rev.* **2020**, *14*, 2000037. [[CrossRef](#)]
16. Wei, W.Q.; Zhang, J.Y.; Wang, J.H.; Cong, H.; Guo, J.J.; Wang, Z.H.; Xu, H.X.; Wang, T.; Zhang, J.J. Phosphorus-free 1.5 μm InAs quantum-dot microdisk lasers on metamorphic InGaAs/SOI platform. *Opt. Lett.* **2020**, *45*, 2042–2045. [[CrossRef](#)] [[PubMed](#)]
17. Shi, B.; Zhu, S.; Li, Q.; Tang, C.W.; Wan, Y.; Hu, E.L.; Lau, K.M. 1.55 μm room-temperature lasing from subwavelength quantum-dot microdisks directly grown on (001) Si. *Appl. Phys. Lett.* **2017**, *110*, 121109. [[CrossRef](#)]
18. Wan, Y.; Norman, J.; Li, Q.; Kennedy, M.J.; Liang, D.; Zhang, C.; Huang, D.; Zhang, Z.; Liu, A.Y.; Torres, A.; et al. 1.3 μm submilliamp threshold quantum dot micro-lasers on Si. *Optica* **2017**, *4*, 940–944. [[CrossRef](#)]
19. Zhou, T.; Tang, M.; Xiang, G.; Xiang, B.; Hark, S.; Martin, M.; Baron, T.; Pan, S.; Park, J.-S.; Liu, Z.; et al. Continuous-wave quantum dot photonic crystal lasers grown on on-axis Si (001). *Nat. Commun.* **2020**, *11*, 977. [[CrossRef](#)]
20. Ma, J.; Zhou, T.; Tang, M.; Li, H.; Zhang, Z.; Xi, X.; Martin, M.; Baron, T.; Liu, H.; Zhang, Z.; et al. Room-temperature continuous-wave topological Dirac-vortex microcavity lasers on silicon. *Light Sci. Appl.* **2023**, *12*, 255. [[CrossRef](#)]
21. ITU-T. *Characteristics of a Single-Mode Optical Fibre and Cable*; International Telecommunication Union: Geneva, Switzerland, 2016.
22. Understand Fiber Attenuation. Available online: <http://fowiki.com/b/understand-fiber-attenuation/> (accessed on 2 June 2015).
23. Zhu, X.; Cassidy, D.T.; Hamp, M.J.; Thompson, D.A.; Robinson, B.J.; Zhao, Q.C.; Davies, M. 1.4- μm InGaAsP-InP strained multiple-quantum-well laser for broad-wavelength tunability. *IEEE Photonics Technol. Lett.* **1997**, *9*, 1202–1204.
24. Ha, W.; Gambin, V.; Wistey, M.; Kim, S.; Harris, J. Multiple-quantum-well GaInNAs-GaNAs ridge-waveguide laser diodes operating out to 1.4 μm . *Photonics Technol. Lett. IEEE* **2002**, *14*, 591–593. [[CrossRef](#)]
25. Mi, Z.; Bhattacharya, P.K.; Yang, J. Growth and characteristics of ultralow threshold 1.45 μm metamorphic InAs tunnel injection quantum dot lasers on GaAs. *Appl. Phys. Lett.* **2006**, *89*, 153109. [[CrossRef](#)]
26. Wei, W.Q.; Wang, J.H.; Zhang, B.; Zhang, J.Y.; Wang, H.L.; Feng, Q.; Xu, H.X.; Wang, T.; Zhang, J.J. InAs QDs on (111)-faceted Si (001) hollow substrates with strong emission at 1300 nm and 1550 nm. *Appl. Phys. Lett.* **2018**, *113*, 053107. [[CrossRef](#)]
27. Ledentsov, N.N.; Kovsh, A.R.; Zhukov, A.E.; Maleev, N.A.; Mikhrin, S.; Vasil'ev, A.P.; Semenova, E.; Maximov, M.V.; Shernyakov, Y.; Kryzhanovskaya, N.V. High performance quantum dot lasers on GaAs substrates operating in 1.5/spl mu/m range. *Electron. Lett.* **2003**, *39*, 1126–1128. [[CrossRef](#)]
28. Kwoen, J.; Imoto, T.; Arakawa, Y. InAs/InGaAs Quantum Dot Lasers on Multi-Functional Metamorphic Buffer Layers. *Opt. Express* **2021**, *29*, 29378. [[CrossRef](#)] [[PubMed](#)]
29. Kwoen, J.; Zhan, W.; Arakawa, Y. E-band InAs quantum dot laser on InGaAs metamorphic buffer layer with filter layer. *Electron. Lett.* **2021**, *57*, 567–568. [[CrossRef](#)]
30. Wei, W.Q.; Huang, J.Z.; Ji, Z.T.; Han, D.; Yang, B.; Chen, J.J.; Qin, J.L.; Cui, Y.O.; Wang, Z.H.; Wang, T.; et al. Reliable InAs quantum dot lasers grown on patterned Si (001) substrate with embedded hollow structures assisted thermal stress relaxation. *J. Phys. D Appl. Phys.* **2022**, *55*, 405105. [[CrossRef](#)]
31. Xu, Z.Y.; Lu, Z.D.; Yang, X.P.; Yuan, Z.L.; Zheng, B.Z.; Ge, W.K.; Wang, J.; Chang, L.L. Carrier relaxation and thermal activation of localized excitons in self-organized InAs multilayers grown on GaAs substrates. *Phys. Rev. B* **1996**, *54*, 11528–11531. [[CrossRef](#)]
32. Anthony, S. *Lasers*; University Science Books: Mill Valley, CA, USA, 1986.
33. Varshni, Y.P. Temperature dependence of the energy gap in semiconductors. *Physica* **1967**, *34*, 149–154. [[CrossRef](#)]
34. Torchynska, T.V.; Hernandez, A.V.; Polupan, G.; Velazquez Lozada, E. Photoluminescence study and parameter evaluation in InAs quantum dot-in-a-well structures. *Mater. Sci. Eng. B* **2011**, *176*, 331–333. [[CrossRef](#)]

Disclaimer/Publisher's Note: The statements, opinions and data contained in all publications are solely those of the individual author(s) and contributor(s) and not of MDPI and/or the editor(s). MDPI and/or the editor(s) disclaim responsibility for any injury to people or property resulting from any ideas, methods, instructions or products referred to in the content.